

A Search for Stellar Populations in High Velocity Clouds

M. H. Siegel¹, S. R. Majewski^{2,3}, C. Gallart⁴, S. Sohn^{2,5}, W. E. Kunkel⁶, R. Braun⁷

ABSTRACT

We report the results of a photometric search for giant stars associated with the cores of four high velocity clouds (HVCs) – two of which are compact HVCs – using the Las Campanas Du Pont 2.5 meter and Cerro Tololo Blanco 4 meter telescopes in combination with a system of filters (Washington M , $T_2 + DDO51$) useful for identifying low surface gravity, evolved stars. Identical observations of nearby control fields provide a measure of the “giant star” background. Our data reach $M_0 = 22$ for three of the HVCs and $M_0 = 21.25$ for the fourth, depths that allow the detection of any giant stars within 600 kpc. Although we identify a number of faint late-type giant star candidates, we find neither a coherent red giant branch structure nor a clear excess of giant candidate counts in any HVC. This indicates that the giant candidates are probably not related to the HVCs and are more likely to be either random Milky Way giant stars or one of several classes of potential survey contaminants. Echelle spectroscopy of the brightest giant candidates in one HVC and its control field reveal radial velocities representative of the canonical Galactic stellar populations. In addition to these null results, no evidence of any young HVC stellar populations — represented by blue main sequence stars — is found, a result consistent with previous searches. Our methodology, specifically designed to find faint diffuse stellar populations, places the tightest upper limit yet on the *total* stellar mass of HVCs of a few $10^5 M_\odot$.

¹University of Texas – McDonald Observatory, Austin, TX, 78712 (siegel@astro.as.utexas.edu).

²University of Virginia, P.O. Box 3818, Charlottesville, VA, 22903
(srm4n@virginia.edu,ss5fb@virginia.edu).

³David and Lucile Packard Foundation Fellow.

⁴Ramón y Cajal Fellow, Instituto de Astrofísica de Canarias 38205 La Laguna, Tenerife, Spain, (carme@iac.es).

⁵Present Address: Korea Astronomy and Space Science Institute, 61-1, Whaam-Dong, Youseong-Gu, Daejeon 305-348, Korea (tonysohn@kao.re.kr).

⁶Las Campanas Observatory, Casilla 601, Las Serena, Chile (kunkel@jeito.lco.cl).

⁷Netherlands Foundation for Research in Astronomy, PO Box 2, 7990 AA Dwingeloo, The Netherlands (rbraun@nrao.nl).

Subject headings: Local Group; Dwarf Galaxies; High Velocity Clouds

1. Introduction

The high velocity clouds (HVCs) are a population of neutral hydrogen clouds with LSR velocities of 80-400 km s⁻¹ (Muller et al. 1963). Despite nearly four decades of study, the nature of the clouds is still a matter of some debate (see, e.g., Wakker & van Woerden 1997; Putman & Gibson 1999) at least partly because of the difficulty in measuring distances to HVCs. Without distances, the nature of the HVCs – e.g., whether they are a Galactic or extragalactic phenomenon – can only be ascertained by indirect means.

It is clear that the dominant HVC feature – the 100° long Magellanic Stream – is the result of interaction between the Magellanic Clouds and the Milky Way, either as a result of tidal disruption or ram-pressure stripping or both (Wannier & Wrixon 1972; Matthewson, Clearly & Murray 1974; Putman et al. 1998, 2003; Putman & Gibson 1999). Some HVCs, particularly Complex C, have been attributed to gas falling onto the Milky Way from similar but perhaps smaller-scale interactions (Larson 1972; Tosi 1988; Gibson et al. 2001; Tripp et al. 2003) while other HVCs are ascribed as the product of Galactic fountains (Shapiro & Field 1976; Bregman 1980, 1996).

The compact high velocity clouds (CHVCs) are possibly the most contentious subset of HVCs. It has been proposed that the CHVCs could be the “missing satellites” of the Local Group (see discussion in Braun & Burton 1999 and 2000, hereafter BB99 and BB00; Blitz et al. 1999; de Heij et al. 2002a; Maloney & Putman 2002; Maller & Bullock 2004), whose existence is presumed on the basis of their formation in N-body simulations of structure formation in the presence of Cold Dark Matter (CDM). These simulations predict the mass distribution of the Local Group to follow a power law $N(M) \propto M^{-\alpha}$ where α is at least 2 (see, e.g., Klypin et al. 1999; Moore et al. 1999). Such a spectrum would imply the existence of several hundred low mass dwarfs in the Local Group, an order of magnitude more than detected, despite a number of optical surveys for low surface brightness members (Mateo 1998; Armandroff et al. 1998, 1999; Karachentseva & Karachentsev 1998, 2000; Karachentsev & Karachentseva 1999; Karachentsev et al. 2000; Whiting et al. 2002; Willman et al. 2004). This contradiction would resolve if the Local Group were filled with dark galaxies – objects containing dark matter but few, if any, stars, perhaps because of inhibition of star formation in the early Universe (see, e.g., Bullock et al. 2000).

The CHVCs’ kinematical preference for the Local Group standard of rest (BB99) and the existence of a small overdensity of clouds toward M31 with high negative velocities (Burton

et al. 2002; de Heij et al. 2002a) suggest Local Group scale distances. High resolution mapping (BB00; Burton et al. 2002) shows several CHVCs to have core-halo morphology, similar to that expected for dark matter-dominated mini-halos. Three independent methods yield distance estimates for some HVCs of $\sim 0.2\text{--}0.7$ Mpc (BB99; BB00; Burton et al. 2001; Robishaw et al. 2003). The CHVCs also show velocity gradients along their major axes with implied rotation speeds of $V_c \sim 15\text{--}20$ km s $^{-1}$ (BB99; BB00; Burton et al. 2001) as well as high internal velocity dispersions. Both phenomena imply high dark matter content (BB00), assuming the HVCs are virialized.

Conversely, the sky distribution of CHVCs appears inconsistent with a Local Group origin (Putman et al. 2002; cf. B99 and de Heij et al. 2002a) and CHVCs are not definitively seen in extragalactic groups (de Blok et al. 2002; Zwann 2001; Banks et al. 1999; Pisano et al. 2004; cf. Braun & Burton 2001). Maloney & Putman (2003) evaluated the effect of extragalactic ionizing radiation on the CHVCs and concluded that the properties of CHVCs are more consistent with a Galactic halo origin than a cosmological one. And while anomalous hydrogen clouds have been found in nearby galaxies (M31; Thilker et al. 2004; M53 and M81; Miller & Bregman 2004), these clouds are closer to their parent galaxies than would be likely for dark galaxies.

One puzzling aspect of CHVCs are the chemical abundances. They are about a tenth solar, a value too low for Galactic fountain models (Wakker et al. 1999; BB99; BB00) but too high for protogalactic fragments, given the lack of recent star formation in HVCs (Blitz et al. 1999; BB99; BB00). It might be consistent, however, with a tidal or ram-pressure stripping origin since many Local Group dwarfs have abundances near this range.

The detection of stars in HVCs would open a new dimension to their study and quickly resolve many uncertainties, including their distance and chemical enrichment history. Additionally, if the CHVCs were discovered to have stellar populations while the HVCs did not, this would clearly indicate that different mechanisms were responsible for the formation of the compact and non-compact HVCs.

If the HVCs were within one Mpc of the Milky Way, they would have red giant stars bright enough to be detected with modest aperture telescopes. A number of recent studies have searched for HVC stars. Willman et al. (2002) surveyed a small number of HVCs that were included in the Sloan Digital Sky Survey and found no indication of stellar content. Hopp et al. (2003) surveyed only CHVCs, combining deep VLT imaging with data from the 2MASS survey and comparing each CHVC to a nearby control field. The VI data rule out significant stellar content to a distance of 2 Mpc, although they cover small regions of each cloud. The 2MASS data cover much larger areas of sky, but would only detect giant stars to a distance of 300 kpc. The most complete survey, by Simon & Blitz (2002),

also focused on CHVCs and failed to detect any stellar content. This study placed a lower limit of 100 kpc on the distance to 250 CHVCs and even greater lower limits (300-1400 kpc) on the distance to 60 CHVCs. The Simon & Blitz survey searched POSS plates for enhancements of stellar density at the positions of the CHVCs and followed up potential detections with monochromatic observations in the Spinrad R_s filter. Though impressive in scale, the Simon & Blitz survey was biased toward larger HVC stellar populations with densities that could rise above the statistical noise of the foreground of Milky Way stars. Diffuse, low surface brightness systems are a much greater challenge to identify against the Poissonian noise of dense foreground/background Galactic starcounts. To find such structures requires observational strategies that increase their detectability.

In this article, we present the first search for *low surface-brightness* stellar populations in HVCs, a search based on the observational strategy of minimizing the effects of Galactic contamination. Our photometric survey of four HVCs and adjacent control fields utilizes a filter system especially sensitive to red giant/supergiant stars — the primary stellar type sought in distant HVCs (and a stellar type found in stellar populations of all ages and metallicities) — and that allows a large fraction of Galactic stellar contaminants — which will be dominated by main sequence stars — to be identified and eliminated. The substantially reduced background/foreground makes it possible to look for very tenuous CHVC stellar populations that would be swamped within simple starcount analyses. For one of our target HVCs and control fields we supplement our photometric analysis with radial velocities derived from echelle spectroscopy of the brightest giant star candidates. §2 of this paper details the observation and reduction of our photometric observations. §3 presents an analysis of these data and attempts to quantify the residual sources of possible “noise” in our program after elimination of the bulk of the likely Galactic dwarf stars. §4 details the spectroscopic work on the brighter giant candidates in one of the HVCs, work that confirms the basic analysis of §3. §5 defines the limits that our survey places on the distances of any stellar populations in the HVCs.

2. Observations and Reduction

The high velocity clouds HVC 017-25-218, HVC 030-51-119 and HVC 271+29+181 were observed in the Washington C , M , and T_2 filters as well as the MgH+Mgb triplet sensitive *DDO51* filter on UT 5-8 June 2000. We used the Du Pont 2.5 meter telescope and the Wide Field Camera (WFC) designed by Ray Weymann and collaborators. The WFC has a circular field of view of 23' at a pixel scale of $\sim 0''.7$ per pixel. The optical defect in the WFC noted by Majewski et al. (2000a) was corrected prior to the observations, providing

a useable, but still modest quality point spread function (PSF) over the entire image (see below). Each HVC was paired with a control field displaced by $\sim 2\text{-}3$ degrees at nearly constant Galactic latitude and observations were switched back and forth between the HVC and control, resulting in identical depth and image quality for each target and paired control field. Total exposure times for each HVC and its control field were 11500-13400 seconds in *DDO51*, 10000-11000 seconds in *C*, 1830-2130 seconds in *T*₂ and 2730-2790 seconds in *M*, integration times that provide completeness in all four passbands to beyond $M = 22$. HVC 030-51-119 and its control field were only minimally observed in *C*.

We observed the high velocity cloud HVC 267+26+216 with the Blanco 4-m Telescope and Mosaic II 8k \times 8k CCD at CTIO during the nights of UT 26-27 February, 2000. The CCD array has a pixel scale of 0''.27 per pixel resulting in a field of view of 37'. The HVC and control field were observed with total exposure times of 300 seconds in *M* and *T*₂, and 2100 seconds in *DDO51*. No data were obtained in *C* for this HVC.

Detailed radio properties of the observed HVCs are listed in B99. Figure 1 shows HIPASS (Barnes et al. 2001, Putman et al. 2002) radio images of the four target HVCs with the test and control fields marked. Coordinates and average reddening coefficients (from Schlegel et al. 1998) for the four HVCs and their control fields are listed in Table 1. We note that the control fields for HVC 017-25-218 and HVC 030-51-119 are not ideally placed. They were positioned before HIPASS (Barnes et al. 2001, Putman et al. 2002) maps became available and unfortunately landed on the extended structure of the target HVCs. However, the locations of the control fields have much lower column densities than the central fields and should still provide a useful contrast to the cores. Analysis of the HIPASS data indicates that HVC 017-25-218 and HVC 271+29+181 meet the definition of *compact* high velocity clouds.¹

Reductions were carried out through the standard IRAF² CCDRED and MSCRED pipelines as appropriate to each data set. The WFC produces a roughly circular image on the square CCD chip. The unexposed areas of the chip consist entirely of CCD noise and can render normal pipeline analysis difficult. We produced an image mask from the flat fields to remove these sections from analysis. The location of the unexposed region of the

¹At the time of our optical observations, HVC 030-51-119 and HVC 267+26+216 were classified as CHVCs. Later radio observations by HIPASS revealed a less compact structure than previous radio images, so that these two objects would no longer be considered CHVCs. In this paper we have reclassified these two objects as HVCs.

²IRAF is distributed by the National Optical Astronomy Observatories, which are operated by the Association of Universities for Research in Astronomy, Inc., under cooperative agreement with the National Science Foundation.

chip, however, varied slightly over the course of the run. As a result, the unexposed regions occasionally extended beyond the nominal mask. These “noisy edges” were generally small ($\leq 0.5\%$ of the total chip area) but produced hundreds of “detections” during photometry. The detections from the noisy edges were clearly non-stellar and were easily removed by our stringent morphological classification (see §3). A re-analysis of our data with more restrictive masking that excludes more of the field edges showed no change in the starcount density.

We derived photometric measures with the DAOPHOT/ALLFRAME PSF photometry package (Stetson 1987, 1994). The PSFs were fit with a quadratically varying Moffat function. The Du Pont data produce modest quality PSFs, with typical rms residuals of 5-7% per pixel. The Blanco images exhibit excellent PSFs, with typical rms residuals of 1-2% per pixel.

All photometry is calibrated to the standard stars of Geisler (1990, 1996) using the matrix inversion and iterative techniques to derive and apply transformation equations described in Siegel et al. (2002). For the Du Pont data, both program and standard stars are measured in identical $3 \times FWHM$ circular apertures. The Blanco MOSAIC data are calibrated using curve-of-growth analysis from DAOGROW (Stetson 1990). The uncertainty in the photometric transformations is approximately 0.01 magnitudes in all filters.

We derived astrometry for our stars from the reference frame of the USNO-A2.0 catalogue (Monet et al. 1996) using the STSDAS TFINDER program in IRAF. Reddening values were generated for each individual star based on interpolation of the reddening maps of Schlegel et al. (1998).

Final photometric catalogues are available in electronic form from the Astrophysical Journal. The catalogues list the photometric measures for stars (as selected in §3) and include $(\alpha, \delta)_{J2000.0}$, photometric measures and E_{B-V} reddening measures. We have also included measures of a modified Welch-Stetson (1993) variability index in which non-variable stars would have values ≤ 1.0 . The 4-meter data only have one observation in each filter and the variability indices are listed as 0.0. The stars from the 2.5-meter data generally have indices ≤ 1.0 indicating little variability over the three days of our observing program and agreement between the formal errors and empirical scatter of the photometric measures. Bright stars are occasionally saturated on the CCD images, resulting in elevated variability indices.

3. Analysis

The M , T_2 , $DDO51$ filter system is now well-established for its ability to distinguish late-type high surface gravity dwarf stars from late-type, low surface gravity, evolved giant stars through the use of two color diagrams (Majewski et al. 2000a,b; Siegel et al. 2000; Palma et al. 2003; Sohn et al. in prep.; Westfall et al. in prep). In particular, we reference Figure 5 of Palma et al. (2003) and Figure 5 of Majewski et al. (2000a), which demonstrate expectations for the appearance of a red giant branch (RGB) in the two-color diagram.

Our data reach a magnitude or more deeper than $M \sim 22$. However, data fainter than $M \sim 22$ have larger uncertainties and less reliable morphological classification. We can reliably classify objects brighter than $M_0 = 22.0$ for the Du Pont data and $M_0 = 21.25$ for the Mayall data³. Figure 2 shows the run of photometric error with magnitude for our data. We apply magnitude error limits to remove obviously poor measures but retain the bulk of the stars. The adopted magnitude error limits are σ_{T_2} , σ_M and $\sigma_{DDO51} < 0.06$ for the Du Pont data and σ_{T_2} , σ_M and $\sigma_{DDO51} < 0.035$ for the Mayall data.

Figure 3 shows color magnitude diagrams (CMDs) of our four HVCs and their corresponding control fields. Because they are at similar Galactic latitudes, are dominated by Milky Way stars, and have identical quality data, the HVC and control field CMDs look similar.

The CMDs clearly show that the HVCs fields do not contain young stars (at least if they are closer than a few hundred kpc, a limit that depends on the age of the main sequence turnoff [MSTO]) since no obvious main sequences project blueward of the “blue edge” of the old, metal-poor halo stars at $(M - T_2) \sim 0.75$. (The slight blueward shift of the blue edge at faint magnitudes is a result of the transition to the more metal-poor populations of the inner halo and thick disk.) This is not altogether surprising, since the previous optical searches of HVCs (B99; B00; Simon & Blitz 2002) have already placed tighter constraints on the absence of young stars in HVCs than our data by virtue of the greater number of clouds surveyed, deeper photometry and/or larger spatial area.

The principal advantage of our program is the degree to which we can detect old or intermediate age stellar populations — particularly very diffuse ones. Such populations would have RGBs well redward of the blue edge. Ordinarily, with simple starcount techniques, a weak RGB might easily be swamped by the foreground of red Galactic dwarf stars and fall

³We classify stars based on the DAOPHOT SHARP parameter. For the 2.5-meter data, objects with $-0.5 < SHARP < 0.11$ are classified as stars; for the 4-meter data, the criterion was $-0.2 < SHARP < 0.11$. See Siegel et al. (2002) for a discussion of the efficacy of DAOPHOT parameters for object classification.

below the detection threshold of the previous surveys. Our program overcomes this problem by severely reducing the Galactic foreground.

The basic premise of the three-filter selection method is that late-type giants and dwarfs occupy different loci in color-color space (Fig. 4). The dwarf stars lie along the arc of stars at negative $M - DDO51$ that traces the strength of magnesium absorption as a function of effective temperature in high surface-gravity, main sequence stars. Low surface-gravity giants lie above this curve in general, offset to a degree dependent upon metallicity (Majewski et al. 2000b).

We interactively fit a sixth order polynomial to $(M - DDO51)_0$ as a function of $(M - T_2)_0$ over the limit $0.7 < (M - T_2)_0 < 3.0$. We gradually removed outliers from this function so that it eventually was entirely defined by stars along the dwarf sequence. Once this system was defined, we derived each star's distance from the nominal dwarf function as:

$$\Delta = (M - DDO51)_0 - f(M - T_2)_0$$

where $f(M - T_2)_0$ is the “best-fitting” locus to the dwarf stars in the two-color diagram. We then flagged any star with $1.0 < (M - T_2)_0 < 2.5$ and a positive Δ value greater than three times its photometric error ($\sigma = \sqrt{\sigma_M^2 + \sigma_{T_2}^2 + \sigma_{DDO51}^2}$) as a potential giant.⁴

This approach provides some distinct advantages over previous efforts that used rigidly defined selection regions in color-color space to select giant candidates (see Majewski et al. 2000a,b; Morrison et al. 2001; Palma et al. 2003). First, if the errors are Gaussian, each giant candidate selected by the above method is 99.7% likely to have photometry placing it genuinely outside the nominal dwarf locus. Second, we obtain an immediate analytical estimate for the contamination level as 0.3% of the total number of stars. Third, even if the errors are not Gaussian or are underestimated, the number of stars with *negative* Δ values greater than 3σ gives a second, robust estimate of the photometric contamination level. Finally, by removing the constraints of rigidly defined selection limits, a star with exceptional photometry is flagged as a giant even if only a short distance from the nominal dwarf locus while a star with poor photometry must pass correspondingly more stringent requirements to be selected as a potential giant.

⁴Since the shape of the dwarf star curve will change with age/abundance (see Paltoglou & Bell 1984), using a single fit for all of the dwarf stars is too simplistic. To take out first order effects in the variation of the dwarf locus, we actually measure Δ with respect to the locus as defined by stars within one magnitude of each star's M .

Figure 5 shows the Δ versus M distribution of the stars in our eight HVC and control fields. The trend is roughly linear, with growing dispersion as the faint end. Stars flagged as giants and negative outliers are marked. Figure 6 shows the color-color diagram of our giant and negative outlier stars. Note that the reddest giant candidates are nearly within the apparent dwarf locus. These are stars with exceptionally small photometric uncertainties.

Table 2 lists the number of giant candidates in each HVC and its corresponding control field, while Figure 7 shows the CMDs of the giant star candidates in the HVCs. The advantage of our method becomes immediately obvious from comparing the raw starcounts to giant star candidate counts in Table 2 or by comparing Figure 7 to Figure 3. The screening for giant star candidates reduces the foreground dramatically – by more than an order of magnitude in all eight cases. A 3σ surface brightness enhancement would have to be 60-200 stars strong to show up in the raw starcounts or uncleaned CMD. However, Figure 7 and the last columns of Table 2 would easily reveal the signature of even a handful of HVC RGB stars, with a 3σ surface brightness enhancement corresponding to only 5-25 stars, an order of magnitude improvement in sensitivity.

The HVC fields have a significant number of giant candidates that, on first blush, would appear to show a stellar population in the HVCs. However, the control fields provide a critical second constraint. The HVC fields show no excess of giant candidates over the control fields. In fact, three of the HVC fields have *fewer* giant candidates than their control fields.

The color-magnitude distribution of giant candidates in the HVCs and their corresponding control fields are similar, although they show a number of interesting features. Most of the giant candidates are toward the fainter end of the data, where contamination by extra-galactic objects and photometric errors is most likely. However, CHVC 017-25-218 and its control field also show a diffuse clump of bright stars around $M_0 \sim 15 - 17$. If bona fide giants, these bright stars would be at distances of 40-100 kpc and therefore well within the bounds of the outer Milky Way halo.

There are few giant candidates with colors near the tip of the red giant branch (TRGB) – typically found at colors of $1.8 \leq M - T_2 \leq 2.5$ for the metallicity range $-2.0 \leq [Fe/H] \leq -0.5$ (see Table 5) and no obvious RGB in any of our fields. The only potential TRGB stars are in the control field of HVC 271+29+181. This field shows a clump of stars near $(M_0, (M - T_2)_0) \sim (21.5, 1.9)$ as well as a sprinkling of brighter red stars. The latter we have found to be field star contaminants (see §4) while the latter could be a very distant (> 450 kpc), very dispersed RGB tip.

In any case, it is clear that the HVCs are not host to any significant stellar population — and our discussions and analysis below suggest that they are not likely even to host *meager*

stellar populations. The most likely explanation for the presence of “giant star candidates” in our fields is that these candidates are either field giants from the Galactic halo, or represent contamination of the giant sample by non-giants. We now quantify these contributions and in §4 show that the radial velocity distribution in one of our fields is consistent with that of Galactic field stars.

3.1. Photometric Errors

As discussed above, our new method of giant star selection should provide an immediate evaluation of the photometric contamination of the giant star region in the two-color diagram. Table 3 lists, for each field, the number of contaminants expected given the 3σ selection criterion and the number of stars with negative Δ values greater than 3σ . For several fields, the latter number is significantly greater than the former. This is a result of the modest quality of the WFC PSF. A disproportionate number of the negative Δ stars are located near the chip edges where the quadratic PSF is not quite adequate. We use the greater of the two numbers to represent the level of photometric contamination, thus providing a conservative estimate for the number of *bona fide* giant stars within our candidate sample.

3.2. Subdwarf Contamination

Another potential source of sample contamination is subdwarf stars. Our candidate selection is based on the presumption that the observed weaker magnesium absorption in these stars is due to surface gravity effects. However, very metal-poor ($[Fe/H] \leq -2.0$) halo subdwarfs may contain so little magnesium that their absorption lines are intrinsically weak and therefore insensitive to surface gravity. Such stars would also fall into the giant region of the two-color diagram. Morrison et al. (2001) estimated this contamination level to be small at bright magnitudes but to grow rapidly at faint magnitudes, depending on the (l, b) of the field. Using their Figure 2, we estimate that our fields should each contain approximately ten subdwarfs, with the exception of HVC 017-25-218, which should contain approximately 20 subdwarfs. This could provide a substantial fraction of the excess “giant candidates” in Table 2.

3.3. Compact Galaxies

The light from distant galaxies has a significant, perhaps even dominant contribution, from giant stars (see, e.g. Bershady 1994 and references therein). In addition, at high enough redshifts, the magnesium features can shift out of the *DDO*51 passband, resulting in bluer $M - DDO51$ colors. An examination of the non-compact objects in our photometry shows that they primarily occupy the giant region, a result we have seen in other deep photometry samples that use this filter system. Our structural parameters should limit galaxy contamination. However, *compact, star-like* extragalactic objects, which are expected to contaminate photometric samples at a level of ~ 200 degree $^{-2}$ to $V \sim 21.5$ (Kron et al. 1991), could remain in the sample. Of course, only a small fraction of compact galaxies have colors red enough to fall into our selection region in the two-color diagram.

To estimate the contribution of compact galaxies to the giant star selection region, we took quasar counts from a recent analysis of the Sloan Digital Sky Survey (Richards et al. 2001). We transformed the $M - T_2$ color limits of our giant selection region ($1.0 < (M - T_2)_0 < 2.5$) to approximate $g - r$ colors ($0.4 < g - r < 1.5$) using transformations in Majewski et al. (2000b) and Fukugita et al. (1996). Approximately 10-15% of the Richards et al. sample fall into this color range resulting in a compact galaxy contamination level of 20 – 30 degree $^{-2}$ in each of our fields, which would be three galaxies for each WFC field and nine for the MOSAIC fields.

This estimate would probably be a lower bound for the 2.5-meter data, which reaches a depth of $M_0 = 22.0$ and may suffer from more extragalactic contamination owing to the mediocre PSF and commensurately lower quality morphological classification. On the other hand, it is probably an upper bound for the 4-meter data given its brighter magnitude limit and superior imaging capability. We choose to split the difference and apply a uniform compact galaxy contamination level of five objects per field.

The C band photometry in three of our HVCs provides an observational test of this approximation. These data were obtained because $C - M$ colors would allow us, had we found a coherent RGB in any of our fields, to place constraints on the metallicity of the giant stars using the iso-metallicity lines derived by Geisler et al. (1991). However, the two-color diagram (Figure 8) shows something unexpected. Many of the giant candidates have far bluer $C - M$ colors than even very metal-poor populations. We find that many of the non-compact galaxies in our photometry also occupy this region of color-color space. Moreover, the star-like objects most displaced from the iso-metallicity lines are preferentially nearer to the faint limit of the data – where galaxy contamination is expected to be strongest.

Our interpretation is that some of our faintest giant star candidates are compact galaxies

and fall into the giant region as a result of their composite spectral energy distribution being dominated by giants, or by being at high enough redshift to shift their magnesium features out of the *DDO51* band. The giant candidates that fall along the iso-metallicity lines in figure 8 are far more likely to be bona fide giants or subdwarfs. Significantly, the number of giant candidates substantially removed from the iso-metallicity lines appears to be approximately 1-10 per field, consistent with the number of extragalactic contaminants estimated above.

3.4. Foreground Giants

As mentioned above, the brighter giant candidates are likely from the Galaxy itself. We estimate the number of Galactic field giants for each field by numerically integrating the Fundamental Equation of Stellar Statistics (von Seeliger 1898) using the density laws derived by Siegel et al. (2002, their table 6), and color-absolute magnitude and giant star luminosity functions from Bergbusch & Vandenberg (2001) converted to Washington colors using the formulae in Majewski et al. (2000b). The number of total estimated contributed Galactic giant stars is listed in the fourth column of Table 3. This includes contributions from the inner halo, thick disk and bulge.

Column five of table 3 lists the total combined predicted contamination level by subdwarfs, compact galaxies, photometric errors as well as the contribution of foreground Milky Way giants. Column six lists the difference between the predicted contamination level and the actual number of giant candidates. Although these numbers come with substantial uncertainties, the comparison shows some patterns. HVC 030-51-119 and HVC 267+26+216 appear to have fewer giant candidates than predicted; their control fields match the predictions almost exactly. On the other hand, the two compact HVCs have a clear excess of giant candidates beyond the expected contamination level, an excess matched in their control fields. These discrepancies are larger than the statistical noise of the sample. The potential implications are discussed in §5.

4. Spectroscopy

In order to test the nature of the giant star candidates, we obtained spectra of twelve giant star candidates in CHVC 271+29+181 and its control field on UT January 27-28 2004 using the 6.5-m Clay telescope at Las Campanas with the MIKE spectrograph. CHVC 271+29+181 is one of the two fields in which both the HVC and control field have a clear excess of giant candidates beyond the predicted contamination level.

The resolution of the echelle spectrograph is approximately $R \sim 19,000$ in the red orders. To derive radial velocities, we used three orders extending from the atmospheric bands near 8300 Å to the Calcium IR triplet. Details of the radial velocity measurement technique can be found in Majewski et al. (2004a). In brief, radial velocities were derived using cross-correlation against a “universal” template masked down to a series of lines that confer the most power in the cross-correlation, and eliminating the vast portions of the spectrum that contain mostly continuum and therefore contribute little more than noise in the cross-correlation. Residual systematic offsets in the velocities were calibrated by observations of K giant velocity standards. The HVC radial velocities thus obtained were subsequently corrected for slit-centering errors by a second cross-correlation focused on the atmospheric absorption bands. The resultant precision on the radial velocities from this multi-step process is better than 1 km s⁻¹.

Table 4 presents the heliocentric radial velocities for the brightest giant star candidates in CHVC 271+29+181 and its control field. Also listed in the table is the strength of each star’s correlation peak, a quality indicator from 0 (worst) to 7 (best) of the spectral quality as well as the de-reddened M magnitude and ($M - T_2$) color.

The most important aspect of the radial velocity distribution is the lack of stars at the radial velocity of CHVC 271+29+181 ($v_{r,LSR} = +181$ km s⁻¹; $v_{r,helio} = +191$ km s⁻¹). The star nearest this radial velocity is 25 km s⁻¹ away and is likely to be a star from the Galactic stellar halo. *We believe that none of our spectroscopically observed giant candidates is associated with the HVC.*

§3 and Table 3 indicate that approximately half of the giant candidates in CHVC 271+29+181 are Galactic field stars (subdwarfs, stars with photometric errors and *bona fide* Galactic giants). The origin of the remaining half is unclear. However, our spectroscopic sample is bright and therefore expected to be heavily dominated by Galactic field stars. The excess of giant candidates is more prevalent at fainter magnitudes.

Figure 9 shows the radial velocity distribution of the stars and confirms that these are indeed Galactic field stars. At the (l, b) of CHVC 271+29+181 the heliocentric radial velocities of any Galactic field stars will primarily reflect circular velocity differences. One would expect roughly three groupings of stars: a thin disk contribution near 0 km s⁻¹, a thick disk with a contribution near 50 km s⁻¹ and a halo contribution near 220 km s⁻¹ (see, e.g. Casertano et al. 1990). Figure 9 shows that the radial velocity distribution is roughly consistent with this. The spectroscopically observed stars lie principally between -5 and 115 km s⁻¹ with a couple of stars at higher, halo-like radial velocities, including star 146, which is in retrograde rotation.

It is not surprising that these stars are Galactic field stars. Inspection of Figure 7 shows that the brightest giants in these two fields are either very red or very blue, where the contamination from photometric error and subdwarfs is expected to be the worst. Indeed, five of the six stars in the control field are at the red end and only slightly removed from the dwarf locus in the two-color diagram, which would suggest that using a more rigid cut-off at the red end of the data may be more appropriate in the future.

Of course, the most interesting stars in CHVC 271+29+181 are the faint, moderately red stars that represent the true excess above the expected contamination level, particularly the clump at $(M_0, (M - T_2)_0) \sim (21.5, 1.9)$ in the control field. Future spectroscopy of these stars will help to determine their nature.

5. Discussion

5.1. Limits on the Stellar Content and Distance of the HVCs

Previous searches for stellar populations in HVCs have concluded that there are not significant populations of stars in HVCs. Our survey of four HVCs here, meant to identify diffuse populations of giant stars, suggests that there may not even be *insignificant* populations of stars in HVCs. In §3 and §4 we show that the small number of giant candidates we have identified along the line of sight to each of the HVCs we studied are likely to be field stars from the standard Galactic stellar populations. Our survey cannot, however, rule out the possibility of a stellar counterpart to the HVCs that might be *displaced* from our probes. Our survey probes consist of a single HVC and control field pair for each target and, these imaged fields actually cover a small fraction of each HVC (see figure 1). Were an HVC stellar population *both* spatially concentrated in its radial distribution *and* centered away from the center of the HI gas, we could erroneously infer a lack of stars.

Ram-pressure stripping, tidal stripping and/or supernovae can potentially separate gas from stars and the halo abounds with examples. The most famous high velocity cloud – the Magellanic stream – is substantially separated from the stellar population of the LMC. Gallart et al. (2001) argue for association of the Phoenix dwarf with an HI cloud that only partly overlaps the stellar populations. The Sculptor dSph has disconnected clumps of gas at similar velocities (Carignan et al. 1998), although this may be foreground contamination by the Magellanic stream (Putman et al. 2003). It is possible that some of the excess stars in our data, particularly in the control fields, could represent a stellar population displaced from the center of the HI. The aforementioned clump of stars at $(M_0, (M - T_2)_0) \sim (21.5, 1.9)$ in the control field of CHVC 271+29+181 could be the RGB tip of a displaced stellar population.

Only further spectroscopy of the giant candidates can eliminate this possibility.

Although ours is the most sensitive probe so far for diffuse stellar populations, it is important to be clear about the upper limits on HVC stellar populations that our null results place. Though the distance, spatial distribution and mass function of any hypothetical HVC stellar populations are unknown, a few basic assumptions allow us to derive useful order-of-magnitude limits. We first define the distance to which we would be able to detect TRGB stars. We estimated TRGB colors and magnitudes from the synthetic photometry of Olsheimer (2003) for a variety of old stellar populations. The TRGB $M - T_2$ color and M_M absolute magnitudes are given in Table 5 for various metallicities. Table 5 also lists minimum distances of a TRGB at which it would be fainter than $M_0 = 22$ and $M_0 = 21.25$.⁵

Beyond 550-760 kpc, RGB stars would be too faint for our program. For an HVC at a hypothetical distance less than these limits, however, we can make a rough analytical approximation of the HVC stellar mass implied by any detected giant stars. At distance D , the absolute magnitude of the TRGB ($M_{abs,TRGB}$) corresponds to an observed apparent magnitude $M_{app,TRGB} = M_{abs,TRGB} + 5\log_{10}\frac{D}{10pc}$. The limiting magnitude of our sample $M_{app,lim}$, in turn, corresponds to an absolute magnitude at distance D of $M_{abs,lim} = M_{app,lim} - 5\log_{10}\frac{D}{10pc}$. An estimate of the number of HVC giant candidates between $M_{app,TRGB}$ and $M_{app,lim}$ allows us to integrate over the luminosity function and spatial distribution of the hypothetical HVC stellar population to estimate a total stellar mass.

The number of stars used for this exercise would optimally be taken from the excess of HVC field stars against control field stars. However, the *deficit* of giant candidates in the HVCs compared with their control fields precludes this. As noted above, however, the two CHVC fields and their control fields have approximately 3 and 7 σ more giant candidates than the predicted contamination level. We therefore calculate implied stellar masses for these two CHVCs by taking the number of giant stars as the lower of either the excess of giant candidates or the total number of stars fainter than $M_{app,TRGB}$. We also run calculations for all four HVCs assuming that only *one* star in the entire sample represented the HVC stellar population. The latter calculation is a useful benchmark of the upper limit to the HVC stellar mass.

We integrate the number of giants over the complete global luminosity function of M3 (Rood et al. 1999), assuming that any local group object would have an LF similar to that of globular clusters (see, e.g., Feltzing et al. 1999). We convert the LF to Washington

⁵We do not expect any of our giant candidates to be red supergiants given the lack of a young main sequence in the CMDs. Post-Asymptotic Giant Branch supergiants could be produced by an old population but are short-lived and therefore rare (see Alves et al. 2001).

colors via the transformations in Majewski et al. 2000b), and assume an exponential spatial distribution with scalelength equal to the HWHM of the HI gas and axial ratio similar to that of the HI gas.

Figure 10 shows the upper limit on stellar mass in the HVCs plotted against distance. The solid lines show the fundamental limitation of our survey. A single HVC star in our sample would imply stellar masses of a few $10^5 M_\odot$. CHVC 017-25-218 is close to its fundamental limit, owing to the comparatively small size of the HVC and the brightness of its excess giant candidates. CHVC 271+29+181 has a higher potential stellar mass ($10^6 M_\odot$). However, this higher mass limit is a result of the large number of faint giant candidates in and large spatial extent of the HVC. We emphasize that these are upper limits and that the CHVC stellar content is likely well below this limit, if it exists at all.

5.2. Halo Streams?

Our predicted giant star candidate counts match the observed counts reasonably well (see table 3). However, the two compact HVCs show an interesting statistical signature. CHVC 017-25-218 and its control field both have approximately 3σ more giant candidates than predicted while CHVC 271+29+181 and its control field have 3σ and 7σ more giant candidates, respectively.

It is unlikely that these stars are associated with the clouds themselves, as shown in the lack of excess in the CHVC central fields over the controls. However, these stars may still be interesting objects in their own right. Our interest is particularly drawn to the clump of stars at $(M_0, (M - T_2)_0) \sim (21.5, 1.9)$ in the control field of CHVC 271+29+191, which could be the tip of a very distant RGB.

One important caveat in the Galactic model used in §3.4, as noted in Siegel et al. (2002), is that the halo often defies conventional density laws. Siegel et al. argued for two halo populations – a smooth inner halo (which we model) and a highly structured outer halo (which we can't and don't), possibly comprised of coherent streams of stellar debris from disrupted dwarf galaxies and/or globular clusters.

Several recent studies using our Washington system have found groups of distant giant stars that are not clearly associated with any known dwarf galaxies or globular clusters. Muñoz et al. (2004) have recently identified a velocity coherent group of halo giants in the line of sight of the Carina dSph galaxy, but which are not associated with the core of that object. In a study around the Magellanic Clouds, Majewski et al. (in preparation; see also Majewski 2004) show that, at large Galactocentric distances, the Galactic stellar

halo may be *dominated* by coherent streams of stars, presumably tidally stripped by the Milky Way from dwarf galaxies or globular clusters. The Majewski et al. fields do *not* show clear RGB structure in the CMD because the streams are diffuse – a result eerily similar to what we have found in our two CHVC fields. Additionally, Ostheimer’s (2002) deep Washington photometry survey of M31 uncovered numerous examples of potentially *intergalactic* giant star candidates, as well as one coherent halo substructure at a distance of about 20 kpc (Majewski et al. 2004b), now confirmed by a strong MSTO feature in his survey data. Interestingly, even this latter, “Triangulum-Andromeda” structure does not exhibit a strongly identifiable RGB in the CMD, but one that is more subtle (Rocha-Pinto et al. 2004). These precedents make it possible to infer that the excesses in the HVC fields may represent distant diffuse star streams in the outer halo that just happen to cross our survey fields.

CHVC 017-25-218 is particularly interesting because its candidate giants are bright. While the HVC and control fields each have approximately twenty giant candidates fainter than $M \sim 19$ — a number consistent with subdwarf, extragalactic and photometric contamination — each of these fields also has approximately forty giant candidates brighter than $M \sim 19$, which is nearly five times the expected contribution from the canonical Galactic models. This field star overdensity could be a signature of halo substructure in the field.

CHVC 017-25-218 is close to the extended stellar stream of the tidally disrupted Sagittarius dSph galaxy (Majewski et al. 2003) and the distance modulus of the Sagittarius stream near this location ($m - M \sim 18$) would put Sgr RGB stars close to the apparent magnitude of the bright clump in CHVC 017-25-218 and its control field. It is highly probable that the excess of bright giants in CHVC 017-25-218 and its control field are giants from the Sagittarius debris stream, although spectroscopy will be needed to confirm this interpretation. If these stars are Sagittarius debris, it validates the basic strategy of our survey since in this case we *would* have successfully identified a diffuse, but distinct stellar population in our fields. It should be noted that even if the stars are Sagittarius debris, this says nothing about the CHVC itself. The radial velocity of CHVC 017-25-218 is a few hundred km s^{-1} discrepant from the Sgr radial velocity near this field.

In §4, we showed that the brighter giants in CHVC 271+29+181 and its control field are Galactic field stars. However, the bulk of the giant candidates are fainter than the limit of our spectroscopy (and fainter than the excess in CHVC 017-25-218 and its control field). It is possible that spectroscopy of the fainter giants — particularly the $(M_0, (M - T_2)_0) \sim (21.5, 1.9)$ group in the control field — might reveal another moving group of giant stars even further into the halo.

6. Summary

Our multifilter examination of four HVCs has failed to detect evidence for a stellar population in four HVCs, which, by virtue of our search strategy for diffuse populations of giant stars, places the strongest limits so far on the existence of stellar populations in the cores of HVCs. Although a number of stars in our survey fields can be classified as distant giants based on their location in two-color space, there is no excess of giant candidates in any HVC compared with its control field. In addition, the total number of giant candidates in our fields roughly corresponds to the predicted contribution from Galactic field stars. Echelle spectroscopy of the brightest giants in one HVC and its control field confirm that they are indeed likely to represent stars from canonical Galactic populations.

The two compact HVCs show a significant excess of giant candidates beyond the predicted contamination level. However, it is likely that these excesses are unrelated to the CHVCs and are, in fact, distant overdensities (perhaps streams) of halo giants unrelated to the HVCs themselves, particularly in CHVC 017-25-218, which nearly overlaps the Sagittarius debris stream. Only further spectroscopy of the giant candidates should definitively resolve these issues.

If none of our stars are associated with their component HVCs, this places an upper limit of a few $10^5 M_\odot$ on the stellar content of the HVCs out to a distance of 0.6 Mpc.

The authors would like to thank J.D. Crane and R.J. Patterson for taking the Mosaic data, J. Rhee and J. Ostheimer for sharing their synthetic photometry for TRGB absolute magnitude calibrations and A. Bernacchi for help reducing the MOSAIC data. This manuscript was much improved by the patient and diligent work of the anonymous referee. The authors also thank M. Putman for helpful discussions. Support for this program was provided to SRM by National Science Foundation (NSF) CAREER Award AST-9702521, NSF grant AST-0307851, the David and Lucile Packard Foundation, a Cottrell Scholar Award from the Research Corporation and a Space Interferometry Mission Key Project grant, NASA/JPL contract 1228235. CG was partially supported by the Spanish Ministry of Science and Technology (Plan Nacional de Investigacion Cientifica, Desarrollo e Investigacion Tecnologica, AYA2002-01939), and by the European Structural Funds.

REFERENCES

Alves, D. R., Bond, H. E. & Onken, C. 2001, AJ, 121, 318
Armandroff, T. E., Davies, J. E. & Jacoby, G .H. 1998, AJ, 116, 2287

Armandroff, T. E., Jacoby, G. H. & Davies, J. E., 1999, AJ, 118, 1220

Banks, et al. 2002, ApJ, 524, 612

Barnes, et al. 2001, MNRAS322, 486

Bershady, M. A. *The Optical and Near-Infrared Colors of Galaxies*, Ph. D. Dissertation, University of Chicago

Blitz, L., Spergel, D. N., Teuben, P. J., Hartmann, D. & Burton, W. B. 1999, ApJ, 514, 818

Braun, R. & Burton, W. B. 1999, A&A, 341, 437 [BB99]

Braun, R. & Burton, W. B. 2000, A&A, 354, 853 [BB00]

Braun, R. & Burton, W. B. 2001, A&A, 375, 219

Bregman, J. N. 1980, ApJ, 236, 577

Bregman, J. N. 1996, in *The Interplay Between Massive Star Formation, the ISM and Galaxy Evolution*, 11th IAP Meeting. Paris: Inst. d’Astrophys. Paris

Miller, E. D. & Bregman, J. N. 2004, *astro-ph/0410238s*

Bullock, J. S., Kravtsov, A. V., & Weinberg, D. H. 2000, ApJ, 539, 517

Burton, W. B., Braun, R., & Chengalur, J. N. 2001, A&A, 369, 616

Burton, W. B., Braun, R. & de Heij, V., 2002, in *High Velocity Clouds*, eds. Wakker, Van Woerden, Schwarz & De Boer, *astro-ph/0206359*

Carignan, C., Beaulieu, S., Côté, S., Demers, S., & Mateo, M. 1998, AJ, 116, 1690

Casertano, S., Ratnatunga, K. U. & Bahcall, J. N. 1990, ApJ, 357, 435

de Block, W. J. G., Zwann, M. A., Dijkstra, M., Briggs, F. H. & Freeman, K. C., 2002, A&A, 382, 43

de Heij, V., Braun, R. & Burton, W. B., 2002b, A&A, 391, 67

de Heij, V., Braun, R. & Burton, W. B., 2002a, A&A, 392, 417

Feltzing, S., Gilmore, G., & Wyse, R. F. G. 1999, ApJ, 516, L17

Fukugita, M., Ichikawa, T., Gunn, J. E., Doi, M., Shimasaku, K., & Schneider, D. P. 1996, AJ, 111, 1748

Gallart, C., Martinez-Delgado, D., Gomez-Flechoso, M. A. & Mateo, M. 2001, AJ, 121, 2572

Geisler, D. 1990, PASP, 102, 344

Geisler, D., Claria, J. J. & Minniti, D. 1991, AJ, 102, 1836

Geisler, D. 1996, AJ, 111, 480

Gibson, B. K., Giroux, M. L., Penton, S. V., Stocke, J. T., Shull, J. M., & Tumlinson, J. 2001, AJ, 122, 3280

Hopp, U., Schulte-Ladbeck, R. E. & Kerp, J. 2003, MNRAS, 339, 33

Karachentsev, I. D. & Karachentseva, V. E. 1999; A&A, 341, 355

Karachentsev, I. D., Karachentseva, V. E., Suchkov, A. A. & Grebel, E. K., 2000; A&A, 341, 355

Karachentseva, V. E. & Karachentsev, I. D., 1998, A&A, 127, 409

Karachentseva, V. E. & Karachentsev, I. D., 2000, A&A, 346, 359

Klypin, A., Kravtsov, A. V., Valenzuela, O. & Prada, F., 1999, ApJ, 522, 82

Kron, R. G., Bershady, M. A., Munn, J. A., Smetanka, J. J., Majewski, S. & Koo, D. C. 1991, in The Space Distribution of Quasars, ed. Crampton, D., ASP Conf. Ser. Vol 21, (San Francisco: ASP), p. 32

Larson, R. B. 1972, Nature, 236, 21

Majewski, S. R., Ostheimer, J. C., Patterson, R. J., Kunkel, W. E., Johnston, K. V. & Geisler, D. 2000a, ApJ, 119, 760

Majewski, S. R., Ostheimer, J. C., Kunkel, W. E., & Patterson, R. J. 2000b, AJ, 120, 2550

Majewski, S. R., Skrutskie, M. F., Weinberg, M. D., & Ostheimer, J. C. 2003, ApJ, 599, 1082

Majewski, S. R., Ostheimer, J. C., Crane, J. D., Siegel, M. H., Palma, C. P., Rhee, J., Kunkel, W. E., Johnston, K. V. & Patterson, R. J. 2004, *in preparation*

Majewski, S. R. et al., 2004, AJ, 128, 245

Majewski, S. R. et al., 2004, ApJ, *in press*, astro-ph/0406221

Majewski, S. R. 2004, ??jnlPASA, 21, 197

Maller, A. H. & Bullock, J. S., 2004, MNRAS, *in press*, astro-ph/0406632

Maloney, P. R. & Putman, M. E. 2003, ApJ, 589, 270

Mateo, M. 1998, ARA&A, 36, 435

Mathewson, D. S., Cleary, M. N. & Murray, J. D. 1974, ApJ, 190, 291

Monet, D. G., et al., 1996, USNO-SA2.0, (Washington: US Naval Obs.)

Morrison, H. L., Olszewski, E. W., Mateo, M., Norris, J. E., Harding, P., Dohm-Palmer, R. C., & Freeman, K. C. 2001, AJ, 121, 283

Moore, B., Ghigna, S., Governato, F., Lake, G., Quinn, T., Stadel, J. & Tozzi, P., 1999, ApJ, 524, 19L

Muller, C. A., Oort, J. H. & Raimond, E. 1963, C. R. Acad. Sci. Paris, 257, 1661

Ostheimer, J. C., 2003, *Exploring the Halo of M31*, Ph. D. Dissertation, University of Virginia

Palma, C., Majewski, S. R., Siegel, M. H., Patterson, R. J., Ostheimer, J. C. & Link, R. P. 2003, apj, 125, 1352

Palma, C., Link, R., Majewski, S. R., Ostheimer, J. C., Frinchaboy, P. M., Patterson, R. J., Kunkel, W. E., Johnston, K. V., & Geisler, D. 2004, AJ, *in prep*

Paltoglou, G. Bell, R. A. 1994, MNRAS, 268, 793

Pisano, D. J., Barnes, D. G., Gibson, B. K., Staveley-Smith, L., Freeman, K. C. & Kilborn, V. A. 2004, ApJ, 610, L17

Putman, M. E., et al., Nature, 394, 752

Putman, M. E. & Gibson, B. K. 1999, Publications of the Astronomical Society of Australia, 16, 70

Putman, M. E., et al., 2002, AJ, 123, 873

Putman, M. E., Staveley-Smith, L., Freeman, K. C., Gibson, B. K. & Barnes, D. G. 2003, ApJ, 586, 170

Richards, G. T. et al. 2001, AJ, 121, 2308

Robishaw, T., Simon, J. D. & Blitz, L. 2003, ApJ, 580, 129L

Rocha-Pinto, H. J. et al., 2004, *in press, astro-ph/0405437*

Rood, R. T., Carretta, E., Paltrinieri, B., Ferraro, F. R., Fusi-Peccci, F., Dorman, B., Chieffi, A., Straniero, O. & Buonanno R., 1999, ApJ, 523, 752

Siegel, M., Majewski, S., & Patterson, R. 2000, BAAS, 197, 134.02

Siegel, M. H., Majewski, S. R., Reid, I. N. & Thompson, I. B. 2002, ApJ, 578, 151

Schlegel, D. J., Finkbeiner, D. P. & Davis, M. 1998, ApJ, 1998, 500, 525

Shapiro, P. R. & Field G. B. 1976, ApJ, 205, 762

Sohn, S., Majewski, S. R., Siegel, M. H. & Patterson, R. J. 2003, *in preparation*

Simon, J.D. & Blitz, L., 2002, ApJ, 574, 726

Stetson, P. B. 1987, PASP, 99, 191

Stetson, P. B. 1990, PASP, 102, 932

Stetson, P. B. 1994, PASP, 106, 250

Thilker, D. A., Braun, R., Walterbos, R. A. M., Corbelli, E., Lockman, F. J., Murphy, E. & Maddalena, R. 2004, *ApJ*, 601, L39

Tripp, T. M. et al. 2003, *AJ*, 125, 3122

Tosi, M. 1988, *A&A*, 197, 47

Wakker, B. P. & van Woerden, H. 1997, *ARA&A*, 35, 217

Wanner, P. & Wrixon, G. T. 1972, *ApJ*, 173, L119

Welch, D. L. & Stetson, P. B. 1993, *AJ*, 105, 1813

Whiting, A. B., Hau, G. K. T. & Irwin, M., 2002, *ApJ*, 141, 123

Willman, B., Dalcanton, J., Ivezić, Z., Schneider, D. P. & York, D. G. 2002,

Willman, B., Governato, F., Delcanton, J. J., Reed, D. & Quinn, T. 2004, *MNRAS*, 353, 639 *AJ*, 124, 2600

Zwann, M. A. 2001, *MNRAS*, 325, 1142

Figure Captions

Fig. 1.— HI column density distribution in the four HVC fields. The HI emission at about $15'$ resolution as observed with HIPASS (Barnes et al. 2001, Putman et al. 2002) from a 7×7 degree field integrated over the velocity extent of each object and scaled to column density assuming negligible HI opacity. The greyscale and contour values are in units of 10^{18} cm^{-2} . The greyscale ranges are indicated by the labeled wedge at the top of each plot. Contours are drawn at 1, 2, 5, 10, 20, 50 and $100 \times 10^{18} \text{ cm}^{-2}$. The overlaid boxes indicate the positions and approximate sizes of the central and control fields observed for each object.

Fig. 2.— Magnitude error as a function of magnitude for all our passbands. DuPont data are on the left, Mayall data on the right. The horizontal lines mark our error limit while the vertical dashed lines indicate the M magnitude limits. The larger uncertainties for the 2.5-meter data reflect the poorer PSF of the WFC more than the smaller aperture.

Fig. 3.— Color-magnitude diagrams of (left, top to bottom) HVC 017-25-218, 030-51-119, 267+26+216, and 271+29+181, along with their corresponding control fields (right, top to bottom). Note the lack of any obvious differences between the HVC and control fields. Note also that any sparse RGB would be swamped by the sheer number of stars in each field.

Fig. 4.— Color-color diagrams of the four HVC fields and control fields. Panels are as in Figure 3. Note the clear separation of the stars into two populations beyond $M - T \sim 1$ – the extended “swoosh” of high-surface gravity dwarfs and the sprinkling of low-surface gravity giant candidates.

Fig. 5.— Giant star selection. The plots show M magnitude against Δ – a measure of the separation of each star from the dwarf locus. Stars are selected as giants (large dots) if they are more than 3σ away from the mean Δ at that magnitude. Starred points are those with $\Delta \leq -3\sigma$ and provide a measure of the photometric contamination level.

Fig. 6.— Color-color diagrams of the four HVC fields and control fields. Panels are as in Figure 2. Large dots are objects selected as potential giant stars based on their Δ values while starred points have $\Delta \leq -3\sigma$ and provide a measure of the photometric contamination level. HVC 267+26+216 shows far less scatter in the two-color diagram because of the shallower limiting magnitude and the superior imaging of the 4-meter telescope.

Fig. 7.— Color-magnitude diagrams of giant candidates selected from the four HVC fields and their control fields. Panels are as in Figure 2. Note the lack of any obvious RGB in the distribution of giant candidates. Note also that most of the candidates are at the faint end of the data, with the exception of HVC 017-225-218.

Fig. 8.— ($C - M$, $M - T_2$) two color diagrams of giant candidates (filled circles) with $\sigma_C \leq 0.08$ from the HVCs and control fields. The dots are dwarf stars. The solid lines are iso-metallicity lines from Geisler et al. 1991. These lines only extend to $M - T_2 = 1.8$. The lines represent (bottom to top) $[\text{Fe}/\text{H}] = -0.5, -1.0, -1.5$ and -2.0 . Note that this two-color diagram compresses surface gravity information. Both dwarf and giant stars will lie along these lines. The gaps between the lines narrows at red colors because the C filter becomes less sensitive to abundance at low temperatures. Many of our giant candidates are well blueward of these lines, indicating that they are not stellar objects. These two-color diagrams can be contrasted with the coherent RGBs shown in Figure 7 of Geisler et al.. The paucity of stars in HVC 030-51-119 and its control field reflects the minimal data obtained in the C filter for those fields.

Fig. 9.— The heliocentric radial velocity distribution of stars in CHVC 271+29+181 and its control field. Overlayed are the approximate radial velocity ranges expected for the canonical thin disk, thick disk and halo velocity distributions from Casertano et al. (1990). Note that the data are roughly consistent with the canonical Galactic stellar populations. Note also the dearth of stars near $+191 \text{ km s}^{-1}$, the heliocentric radial velocity of the CHVC.

Fig. 10.— The upper limit of stellar mass in each of our four HVCs as a function of distance along the line of sight. The rollover at large distances is the magnitude limit of the data.

Table 1. Target Fields

Field	$(\alpha, \delta)_{2000.0}$	(l, b)	E_{B-V}
CHVC 017-25-218	19:59:06.0,-24:55:00	16.6,-25.3	0.107
Control 017-25-218	20:00:18.5,-23:04:03	18.6,-24.9	0.148
HVC 030-51-119	21:58:18.0,-22:42:00	29.6,-50.7	0.044
Control 030-51-119	21:59:55.9,-21:24:01	31.7,-50.7	0.037
HVC 267+26+216	10:28:06.15,-26:40:44.0	267.2,26.2	0.077
Control 267+26+216	10:36:26.18,-27:56:49.5	270.5,26.2	0.061
CHVC 271+29+181	10:48:54.0,-26:23:00	271.5,28.9	0.051
Control 271+29+181	10:57:22.2,-27:29:12	274.0,28.9	0.068

Table 2. Number Counts

Field	$N_{stars,HVC}$	$N_{stars,Control}$	$N_{giants,HVC}$	$N_{giants,Control}$
CHVC 017-25-218	3179	2973	63	60
HVC 030-51-119	555	550	6	22
HVC 267+26+216	1867	1885	10	28
CHVC 271+29+181	1032	1262	35	67

Table 3. Giant Region Contamination

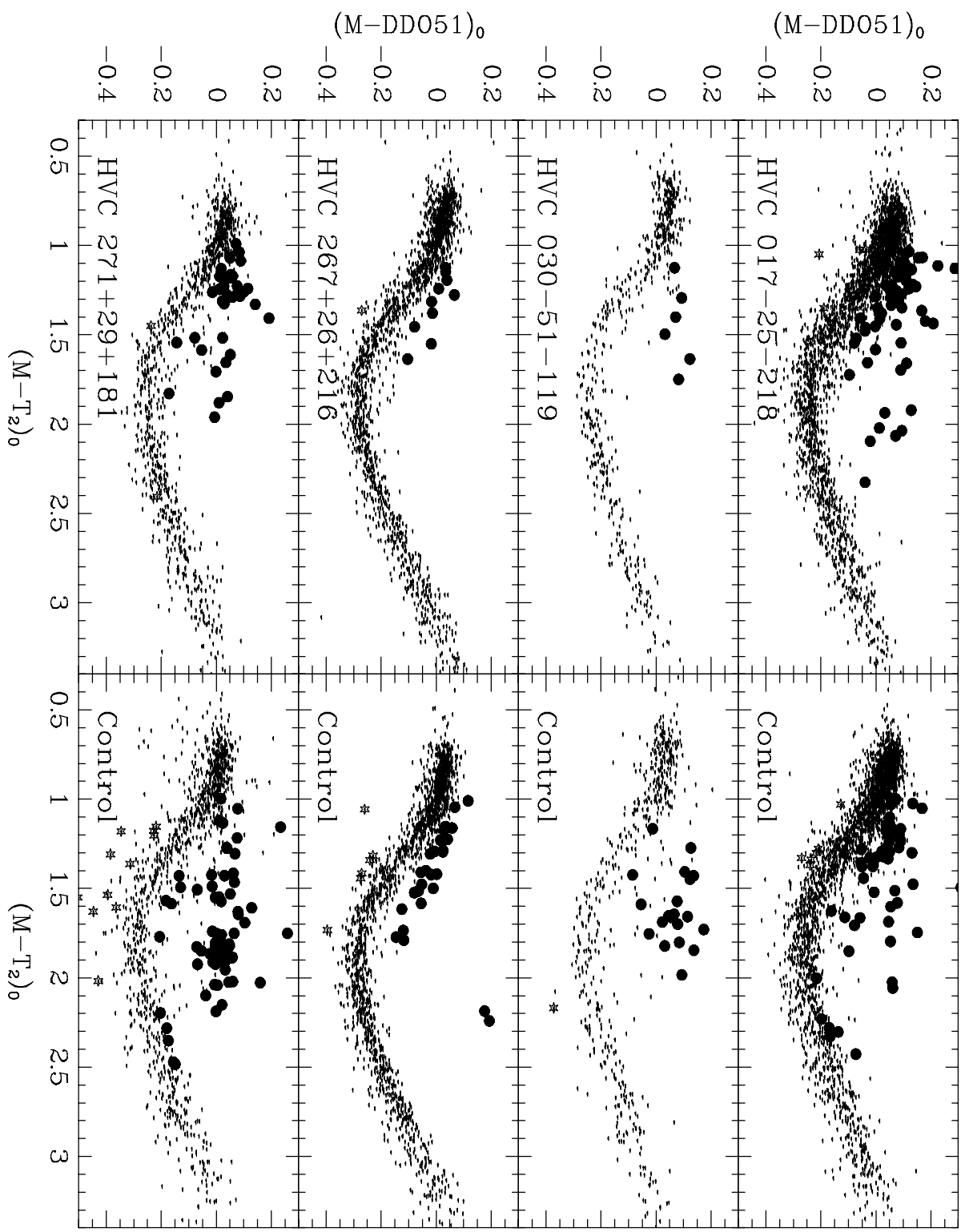
Field	$N_{expected}$	$N_{\Delta \geq 3\sigma}$	$N_{Galactic}$	N_{Total}	N_{Excess}
CHVC 017-25-218	10	4	8	43	20
Control 017-25-218	9	6	8	42	18
HVC 030-51-119	2	0	2	19	-13
Control 030-51-119	2	3	2	20	-2
HVC 267+26+216	6	1	6	27	-17
Control 267+26+216	6	6	7	28	0
CHVC 271+29+181	3	2	2	20	15
Control 271+29+181	4	11	2	28	39

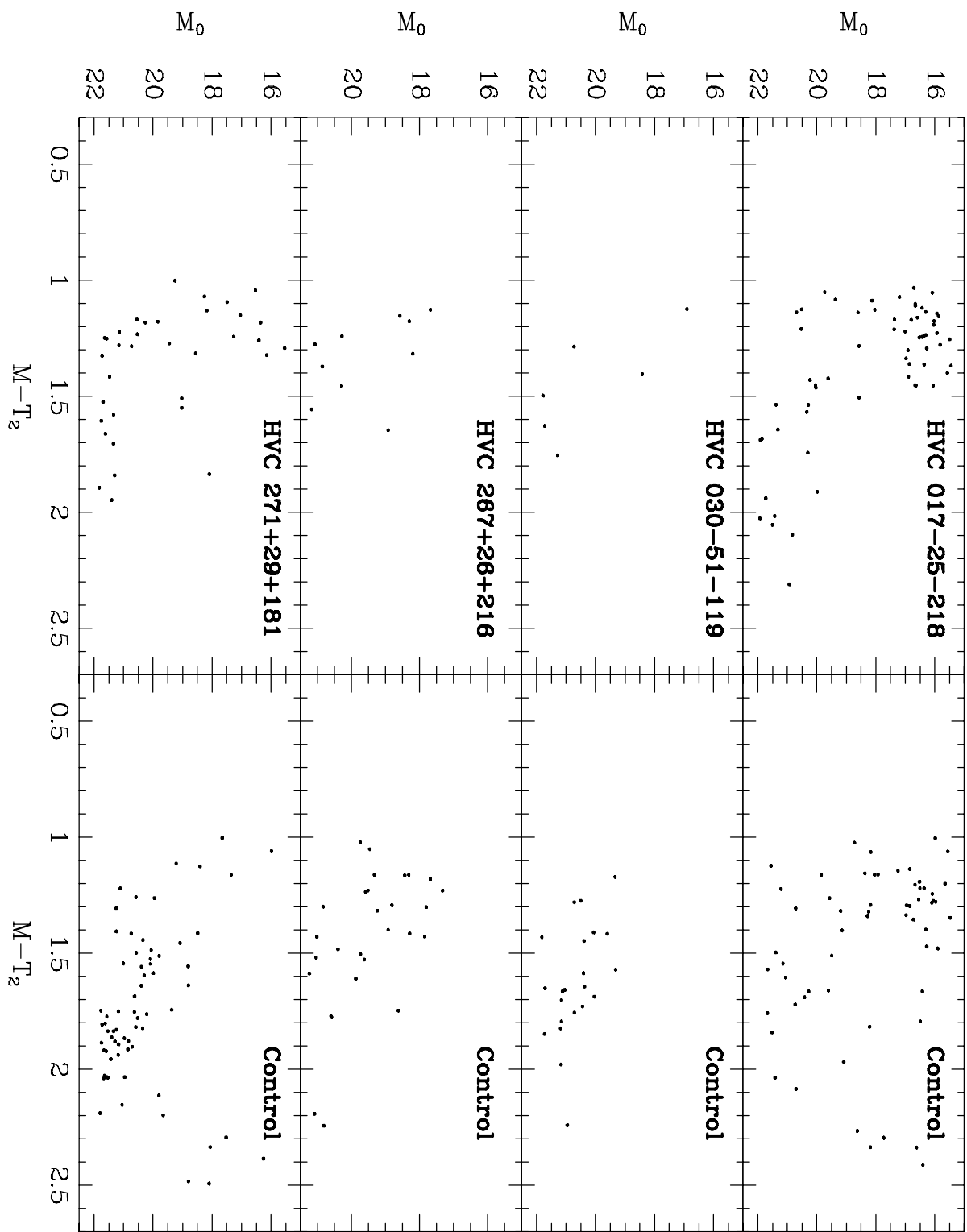
Table 4. Giant Candidate Radial Velocities

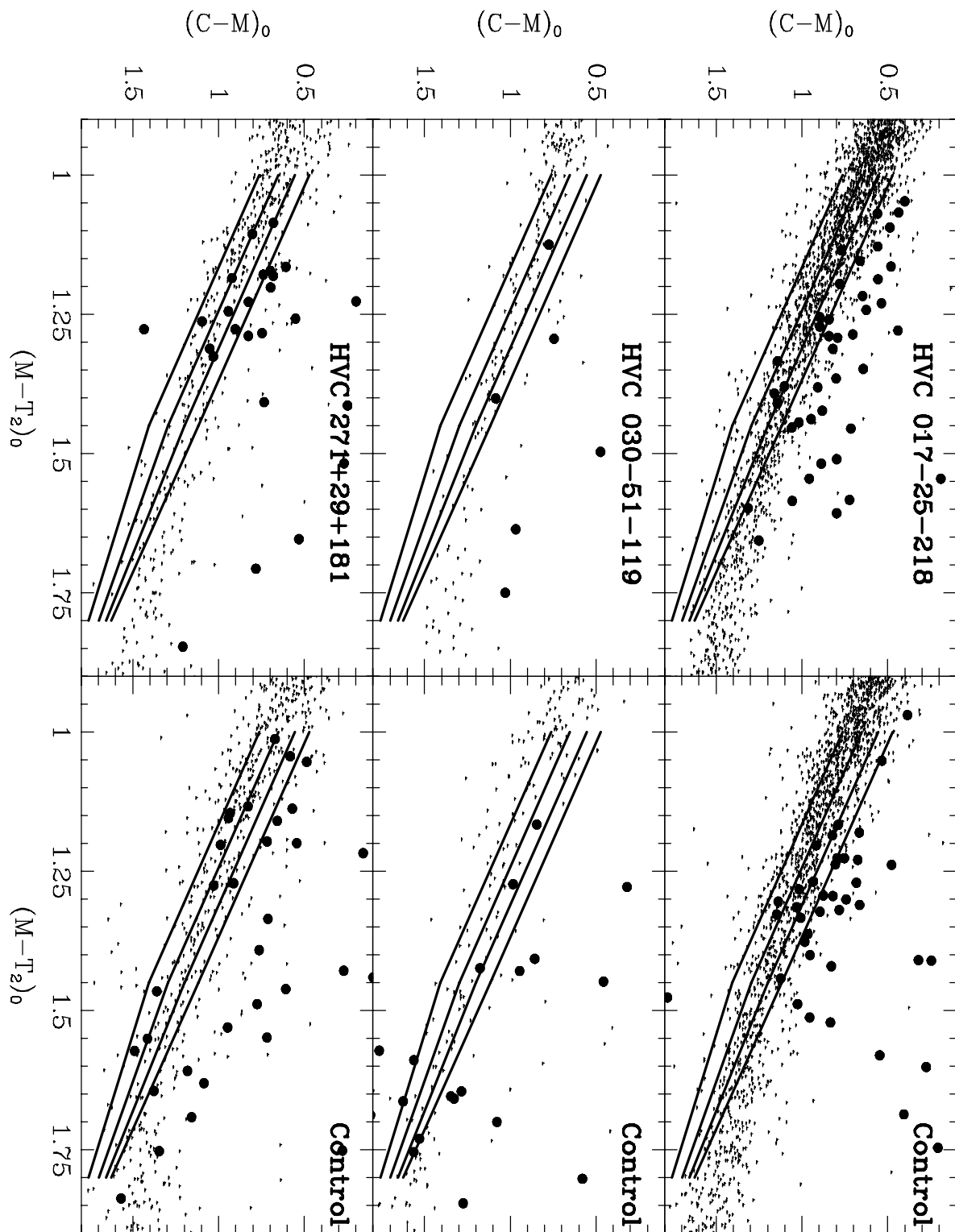
Field	Star ID	$v_{r, helio}$ km s ⁻¹	Correlation Peak	Q (0-7)	M_0	$(M - T_2)_0$
CHVC 271+29+181	240	147.01	0.67	4	17.49	1.09
CHVC 271+29+181	231	85.21	1.01	7	17.27	1.24
CHVC 271+29+181	206	40.55	0.71	6	17.04	1.15
CHVC 271+29+181	160	115.01	1.10	7	16.41	1.26
CHVC 271+29+181	146	349.69	0.82	7	16.53	1.04
CHVC 271+29+181	142	66.76	0.65	7	16.36	1.18
CHVC 271+29+181	126	106.95	0.84	7	16.15	1.32
CHVC 271+29+181	87	-44.42	1.10	7	15.54	1.29
Control 271+29+181	517	24.67	0.66	6	18.10	2.49
Control 271+29+181	445	-8.33	0.83	7	17.52	2.29
Control 271+29+181	134	215.08	0.79	7	15.99	1.06
Control 271+29+181	93	-4.63	1.15	7	16.26	2.38

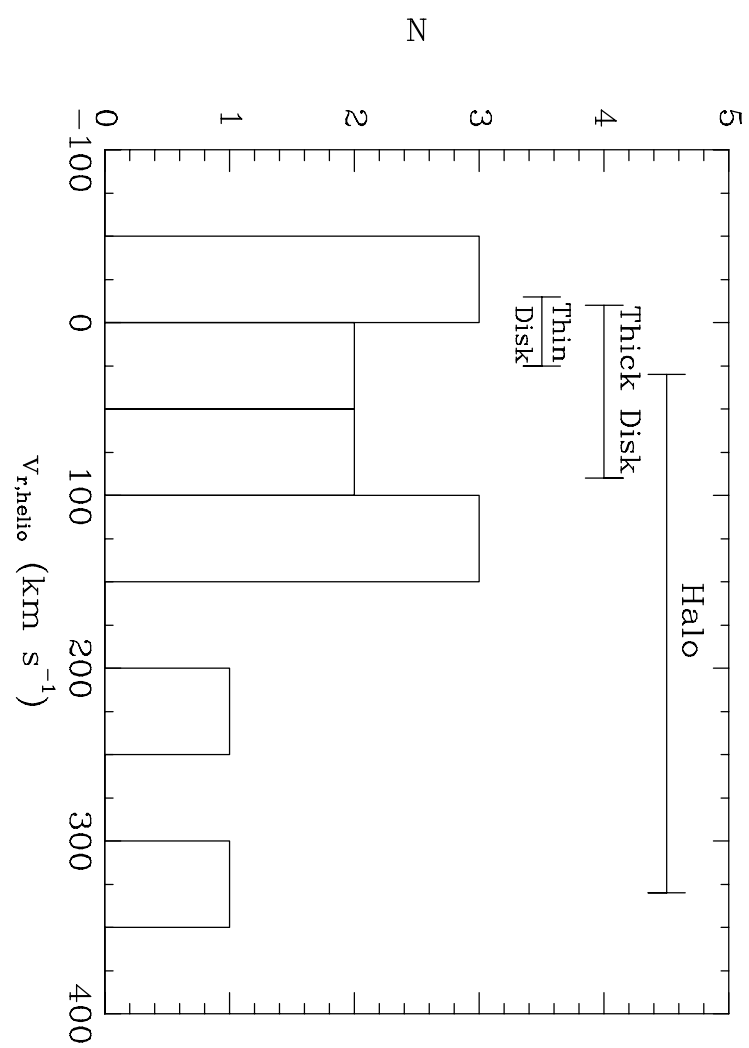
Table 5. HVC Distance Limits

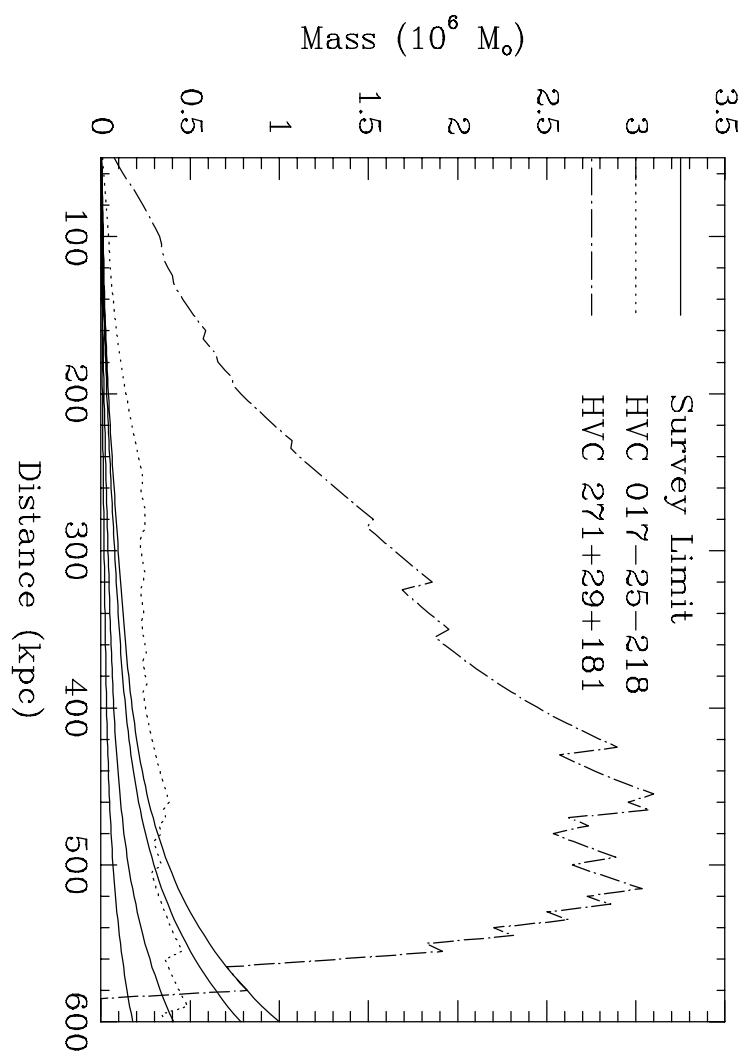
[Fe/H]	Age (Gyr)	$(M - T_2)_{TRGB}$	$M_{M, TRGB}$	$r_{\odot, M=22}$ (kpc)	$r_{\odot, M=21.25}$ (kpc)
-2.0	10-15	1.78	-2.41	760	540
-1.5	10-15	1.94	-2.28	720	510
-1.0	10-15	2.22	-1.99	630	450
-0.5	10-15	2.49	-1.70	550	390











This figure "f1a.jpg" is available in "jpg" format from:

<http://arxiv.org/ps/astro-ph/0412699v1>

This figure "f1b.jpg" is available in "jpg" format from:

<http://arxiv.org/ps/astro-ph/0412699v1>

This figure "f1c.jpg" is available in "jpg" format from:

<http://arxiv.org/ps/astro-ph/0412699v1>

This figure "f1d.jpg" is available in "jpg" format from:

<http://arxiv.org/ps/astro-ph/0412699v1>

This figure "f2.jpg" is available in "jpg" format from:

<http://arxiv.org/ps/astro-ph/0412699v1>

This figure "f3.jpg" is available in "jpg" format from:

<http://arxiv.org/ps/astro-ph/0412699v1>

This figure "f4.jpg" is available in "jpg" format from:

<http://arxiv.org/ps/astro-ph/0412699v1>

This figure "f5.jpg" is available in "jpg" format from:

<http://arxiv.org/ps/astro-ph/0412699v1>